THE ASTROPHYSICAL JOURNAL, 416:563–575, 1993 October 20

STAR FORMATION IN THE SPIRAL ARMS OF NGC 4321. II. H I DISTRIBUTION AND KINEMATICS

JOHAN H. KNAPEN,[1,2] JORDI CEPA,[1] JOHN E. BECKMAN,[1] M. SOLEDAD DEL RIO,[1] AND ALAN PEDLAR[3]
Received 1992 December 21; accepted 1993 April 21

ABSTRACT

We present H I 21 cm observations of the grand design spiral galaxy NGC 4321, as obtained with the VLA. From our original data, we have obtained data cubes with resolutions ranging from 13″ to 45″. The H I is observed to break up into small condensations at high resolution. These condensations, with typical masses of $3.3 \pm 0.7 \times 10^7\ M_\odot$, are not confined to the arm regions. They may be unresolved at 15″ resolution and thus may have physical sizes smaller than 1 kpc. The total H I distribution is mostly confined to the radius of the optical disk, but a large though faint extension is seen in the H I data at 45″ resolution on the SW side of the disk. NGC 4321 is asymmetric in H I and may be called "lopsided." We have derived a rotation curve which agrees fairly well with what was previously published but shows more detail due to the higher resolution of our new observations. The rotation curve does not decline within the radius of the disk, but important differences are seen between the behavior of the approaching and the receding sides. These differences are caused by deviations from circular motions in the outer disk that are probably due to a close passage of the companion galaxy NGC 4322, which may also be the cause of the observed asymmetry in the total H I distribution. Deviations from circular motion due to density wave streaming are seen in the inner disk. From skewing of the velocity contours in the central part of NGC 4321, the presence of a nonaxisymmetric potential is deduced. Near-infrared and Hα images indicate that a bar is indeed present in this galaxy. The deviations from circular motions seen in the velocity field can be identified with gas streaming around the bar in elongated orbits, in broad agreement with theoretical predictions.

Subject headings: galaxies: individual (NGC 4321) — galaxies: kinematics and dynamics — galaxies: spiral — galaxies: structure — radio lines: galaxies — stars: formation

1. INTRODUCTION

An important line of approach in the study of recent star formation processes in disks and spiral arms of galaxies is the observational one using information on the current star formation rate and on the underlying gas density. We are performing an observational study using Hα luminosity as an indicator of massive star formation activity, and column densities of neutral hydrogen gas in both its molecular and atomic form (from CO and H I observations, respectively) to estimate the total gas density. Studying the star formation efficiency in NGC 5194 (M51), we have found that the massive star formation along the main spiral arms is triggered, probably by spiral density waves (Knapen et al. 1992). Using Hα, H I, and CO data taken from the literature, we found that the arm/interarm ratio of Hα luminosity per unit gas mass along the arms shows strong peaks and dips, which do not correspond to similar variations in the neutral gas density. This pattern occurs symmetrically in the two main arms and could be identified geometrically with a pattern of density wave resonances. Cepa & Beckman (1990a) found similar patterns in two grand design spirals studied previously (NGC 628 and NGC 3992).

Knowledge of the H I distribution in a galaxy is important for determining the precise rôle of atomic hydrogen in the star formation process. Comparison with the H_2 (from CO) will indicate which is the dominant phase of the neutral gas inside and outside the arms, and how the ratio of molecular to atomic gas changes radially, both in the arms and in the interarm regions. In the case of M51, about 90% of the total hydrogen in the inner part of the disk of the galaxy is in molecular form (see, e.g., Scoville & Young 1983), and much of the atomic hydrogen, especially in the inner disk, may have been formed from dissociation of molecular gas in regions of massive star formation, as proposed by Allen, Atherton, & Tilanus (1986) and Tilanus & Allen (1989, 1991) and also observed by Knapen et al. (1992).

The velocity field derived from 21 cm line imaging will give information on the different mechanisms which may play a rôle in the enhanced star formation in certain regions of a grand design spiral, such as in the spiral arms or at the ends of a bar. It may allow us to detect deviations from purely circular motions in the velocity field, due to, for instance, density wave streaming or the influence of a nonaxisymmetric potential (e.g., that of a stellar or gaseous bar). Streaming motions have been observed in H I by, e.g., Visser (1980) in M82, and Rots et al. (1990) in M51; and in CO by, e.g., Ichikawa et al. (1985) in M31, Clemens (1985) in the Milky Way, and Cepa et al. (1992) in NGC 4321. Effects of a bar potential on the velocity field have been seen in optical velocity studies by, e.g., Peterson et al. (1978) in NGC 5383 and Pence et al. (1988) in NGC 4027, and in H I by, e.g., Sancisi, Allen, & Sullivan (1979) in NGC 5383, Gottesman et al. (1984) in NGC 3992 and NGC 4731, Ondrechen & van der Hulst (1989) in NGC 1365, and Ondrechen, van der Hulst, & Hummel (1989) in NGC 1097.

For our star formation study, where we specifically compare arm with interarm regions, we need at least enough spatial resolution to resolve an arm. In the case of the galaxy chosen for the present study, NGC 4321, this entails a resolution of

[1] Instituto de Astrofísica de Canarias, E-38200 La Laguna, Tenerife, Spain.
[2] Also Kapteyn Astronomical Institute, The Netherlands.
[3] Nuffield Radio Astronomy Laboratories, Jodrell Bank, Macclesfield, Cheshire SK11 9DL, Great Britain.

about 15″, corresponding to 1.0 kpc at the adopted distance to the galaxy of 13.8 Mpc (de Vaucouleurs 1984; this distance was also adopted by Arsenault et al. 1988). This resolution does not present a problem, of course, for optical observations, but is more difficult to achieve for observations of the neutral gas. In the case of NGC 4321, we have used the NRO 45 m dish for the CO measurements, which yields an angular resolution of 15″ at 115 GHz (first results were presented in Cepa et al. 1992, hereafter Paper I). For the H I study, we had to make new observations with higher angular resolution since both the WSRT (Warmels 1988) and VLA (Cayatte et al. 1990) observations published in the literature have resolutions of about 45″.

The present paper is the second in a series devoted to a major observational study of the star formation efficiency in the grand design spiral NGC 4321 (In Paper I we presented CO observations and an analysis of the kinematics and distribution of the molecular gas). NGC 4321 (M100) is the largest spiral in the Virgo Cluster, 4° from the central Virgo galaxy M87 (corresponding to about 1 Mpc). Its radio continuum emission was studied by van der Kruit (1973) and Kotanyi (1980), both at 1.4 GHz, and at higher resolution by van der Hulst et al. (1981) and Weiler et al. (1981), at 4.9 GHz. The H I content and its distribution in NGC 4321 were described earlier at 45″ resolution by Warmels (1988) and Cayatte et al. (1990). Arsenault et al. (1988) published a velocity field derived from Fabry-Perot observations of the Hα line, and Cepa & Beckman (1990b) presented a statistical study of the distribution of H II regions as measured from an Hα image. The H I and Hα line velocity studies show some evidence of nonaxisymmetric motions in the central part of the galaxy, which may be due to a bar. The existence of this bar is not obviously apparent in optical images; Sandage & Tammann (1987), for instance classified NGC 4321 as Sc, whereas de Vaucouleurs, de Vaucouleurs, & Corwin (1976) classified it as a barred spiral, of type SABbc.

Here we report our new observations of the H I content and kinematics of NGC 4321, obtained with the Very Large Array. We compare the H I data with optical images in the *I*-band and in Hα obtained at La Palma. We present evidence from kinematics and morphology that NGC 4321 is in fact a barred spiral. In § 2 of this paper we give the details of the observations and the data reduction. In § 3 we describe the distribution of the neutral hydrogen gas. In § 4 the H I kinematics of NGC 4321 are discussed and the rotation curve is derived and compared with other determinations published in the literature. We compare the morphology in optical broad-band and Hα images with the H I data in § 5 and discuss the possible orientation and gas flows in the bar of the galaxy. The main conclusions are summarized in § 6.

2. OBSERVATIONS AND REDUCTION

We observed NGC 4321 twice in the 21 cm line of neutral hydrogen with the Very Large Array (VLA)[4] of the National Radio Astronomy Observatory: first in the D (1 km; 44″ angular resolution), and later in the C (3 km; 12.″5 resolution) configuration. The observing parameters are summarized in Table 1. The galaxy was observed for 12 hr in each of the configurations, on 1990 January 14 in D and on 1990 November 27 in C. Using the standard AIPS reduction procedures, we combined these observations and produced maps with a resolution of 12.″7 × 13.″3 (uniform weighting) and 31.″75 × 28.″75 (natural weighting). Note that the lack of spacings shorter than 33 m will affect only structures larger than some 10′ and that our NGC 4321 measurements will therefore not be affected. As a check, we convolved the images from the uniformly weighted data set to the resolution of the images from the naturally weighted data, showing that there were no significant differences, apart from the higher noise in the uniform maps. We used the uniform maps in most of the present study since we are interested in high spatial resolution and used the natural maps only to study the H I distribution in the outer parts of the galaxy. The velocity range covered by the observations is 1333 km s^{-1}, with a velocity resolution of 20.83 km s^{-1}. The central velocity was 1575 km s^{-1}.

TABLE 1

VLA OBSERVATIONAL PARAMETERS

Parameter	Value
Target	NGC 4321
Observing dates	1990 Nov 27 (C array) 1990 Jan 14 (D array)
Field Center:	
R.A.(1950)	$12^h20^m22^s.9$
Decl.(1950)	16°06′00″
Shortest spacing	0.033 km
Longest spacing	3.4 km
Number of antennas	26
F.W.H.P. primary beam	30′
Central velocity channel	1575 km s^{-1}
Number of channels	64
Velocity resolution	20.83 km s^{-1}

The continuum emission was determined by averaging 10 channels free of line emission on the low-velocity side and 13 at the high-velocity side of the data cube. The result was subtracted from all the channel maps containing line emission. After Hanning smoothing, it was noted that only 19 channels contained detectable H I; hence, only these channels were included in the final data cube.

We convolved the uniformly weighted data set with Gaussian beams and obtained four sets of channel maps, with resolutions of 12.″7 × 13.″3, 15″, 20″, and 30″. These continuum-free channel maps were cleaned using the AIPS APCLN task, based on the algorithm described by Clark (1980). The cleaning was repeated for all the separate cubes obtained from the original one after convolving with a Gaussian beam. Using the same procedure we produced 45″ resolution channel maps from our naturally weighted data set. The sensitivities of the cleaned data sets at the various resolutions are given in Table 2.

The cleaned channel maps at 20″ resolution are shown in Figure 1*a*, and Figure 1*b* shows the channel maps at 45″

TABLE 2

MAP PROPERTIES

Synthesized Beams (FWHM)	rms Noise (mJy beam^{-1})	$T_b(K)/S$ (mJy beam^{-1})
13.″31 × 12.″73	1.0	3.55
15″ × 15″	1.0	2.67
20″ × 20″	0.8	1.31
30″ × 30″	0.65	0.67
(Natural) 31.″75 × 28.″75	0.50	0.64
(Natural) 45″ × 45″	0.67	0.30

[4] The National Radio Astronomy Observatory is operated by Associated Universities, Inc., under cooperative agreement with the National Science Foundation.

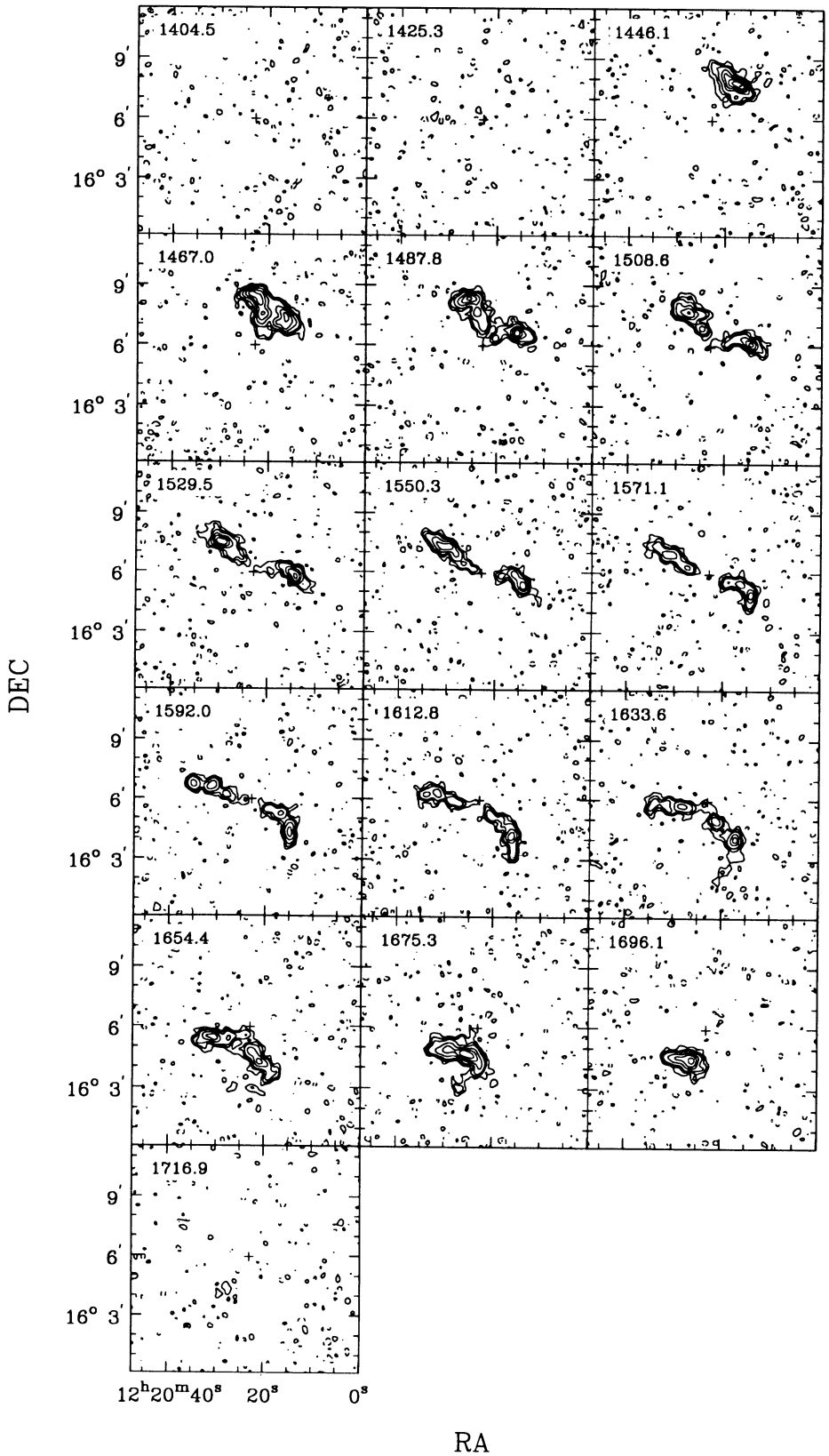

FIG. 1*a*

FIG. 1.—(*a*) Channel maps of the continuum-subtracted H I line emission for NGC 4321, at 20″ resolution. Contour levels are at −3.2, −1.6 (*dashed*), 1.6 (= 2 σ), 3.2, 4.8, 8.0, 11.2, 14.4, 17.6, and 20.8 mJy beam^{-1}. The optical center of NGC 4321 is indicated with a cross. The heliocentric velocity of each map is shown in the upper left-hand corner. (*b*) Channel maps at 45″ resolution. Contour levels are at −3.0, −2.0, −1.0 (*dashed*), 1.0 (= 1.5 σ), 2.0, 3.0, 4.0, 6.0, 8.0, 12.1, 16.1, 20.1, 26.8, and 40.2 mJy beam^{-1}. The optical center is indicated with a cross, and the beam size as a hatched ellipse in the last panel. The heliocentric velocity of each map is shown in the upper left-hand corner.

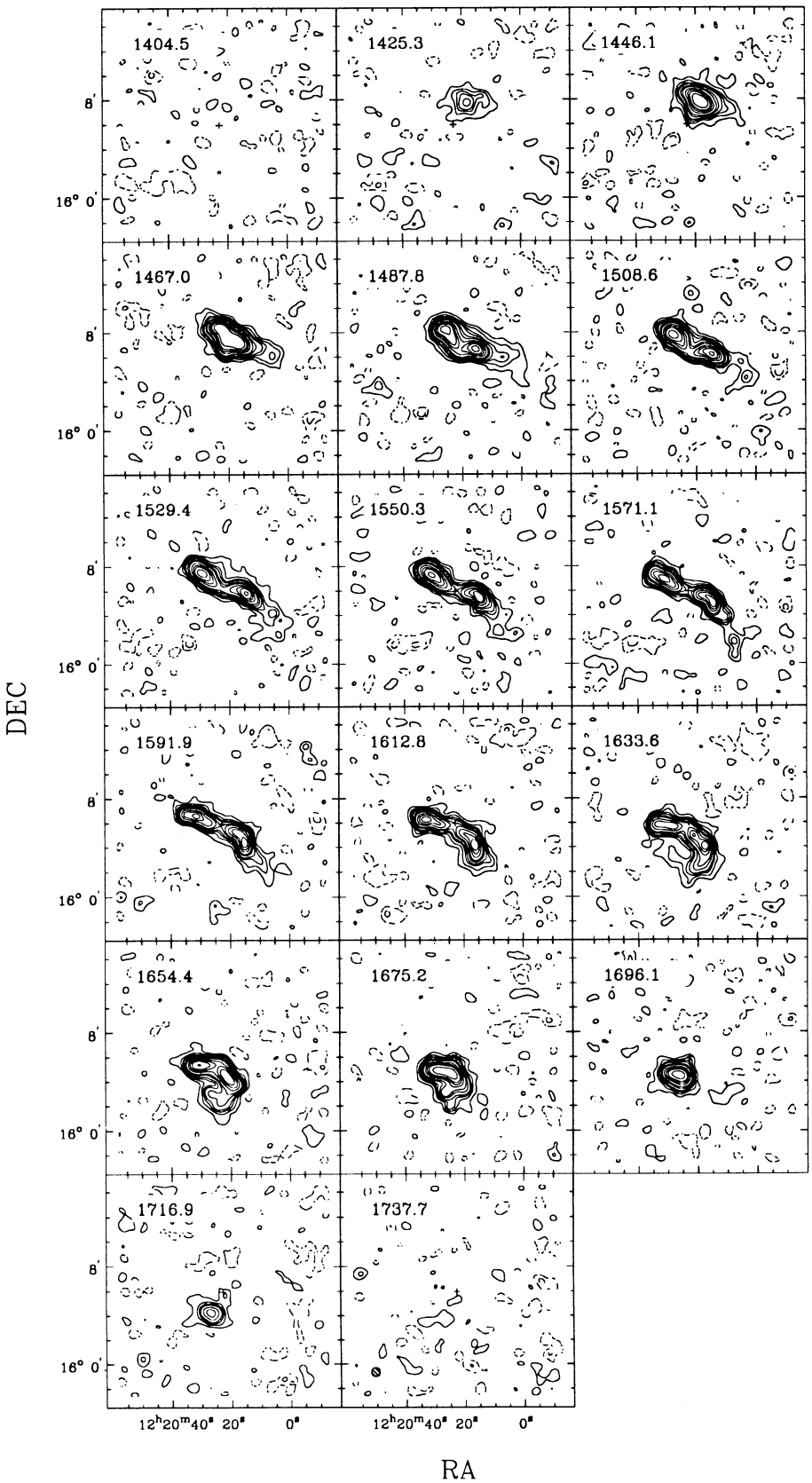

FIG. 1*b*

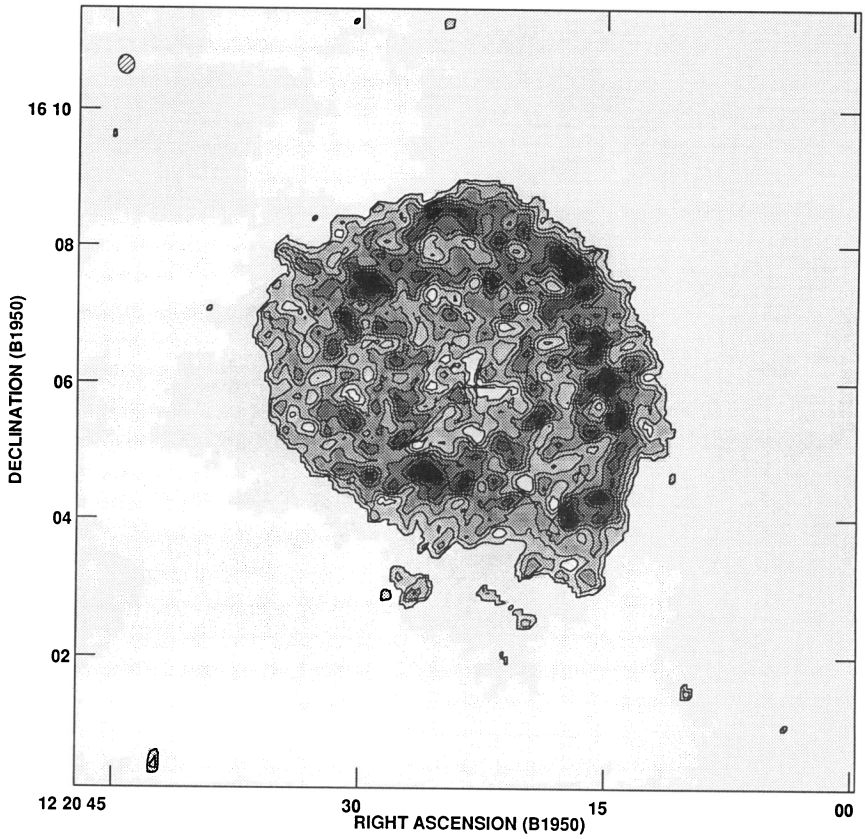

FIG. 2a

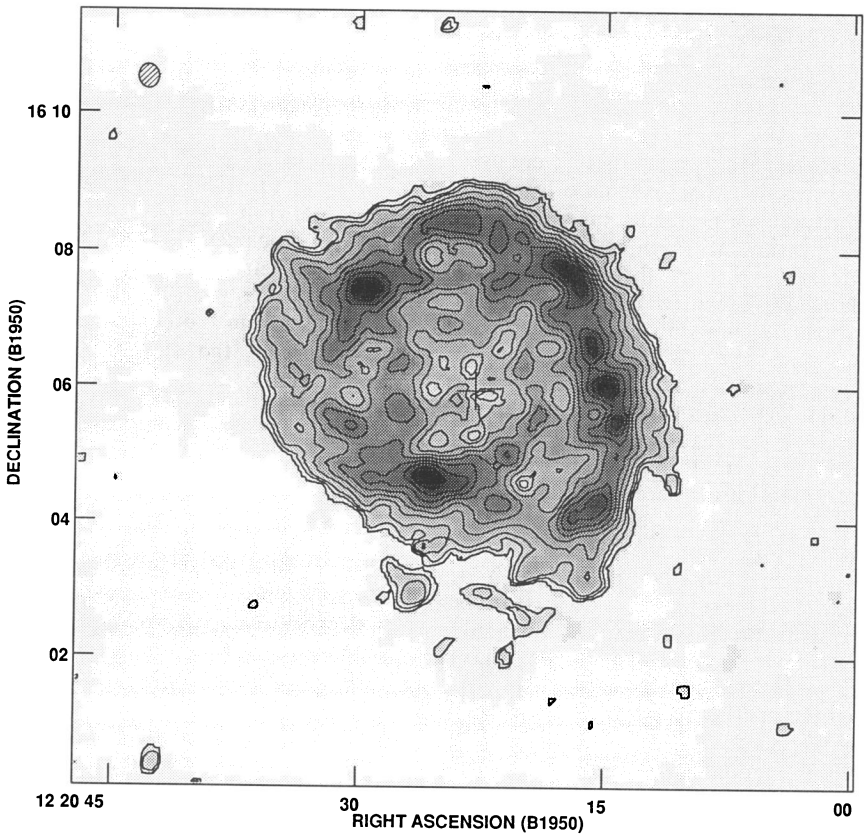

FIG. 2b

FIG. 2.—(*a*) Distribution of total H I column density (zeroth moment map) at 15″ resolution. Contour levels are from 0.98 to 14.7 in steps of 1.95×10^{20} atoms cm^{-2}, The cross represents the optical center of NGC 4321. Contour plot is shown overlaid on gray-scale representation of the same image. Beam size is indicated in the upper left-hand corner. (*b*) As in (*a*), at 20″ resolution. Contour levels are 0.96, 1.92×10^{20} atoms cm^{-2} and from 2.88 to 16.3 in steps of 1.92×10^{20} atoms cm^{-2}. (*c*) As in (*a*) at 45″ resolution. Contour levels are 0.27, 0.82×10^{20} atoms cm^{-2} and from 1.37 to 9.61 in steps of 1.37×10^{20} atoms cm^{-2}.

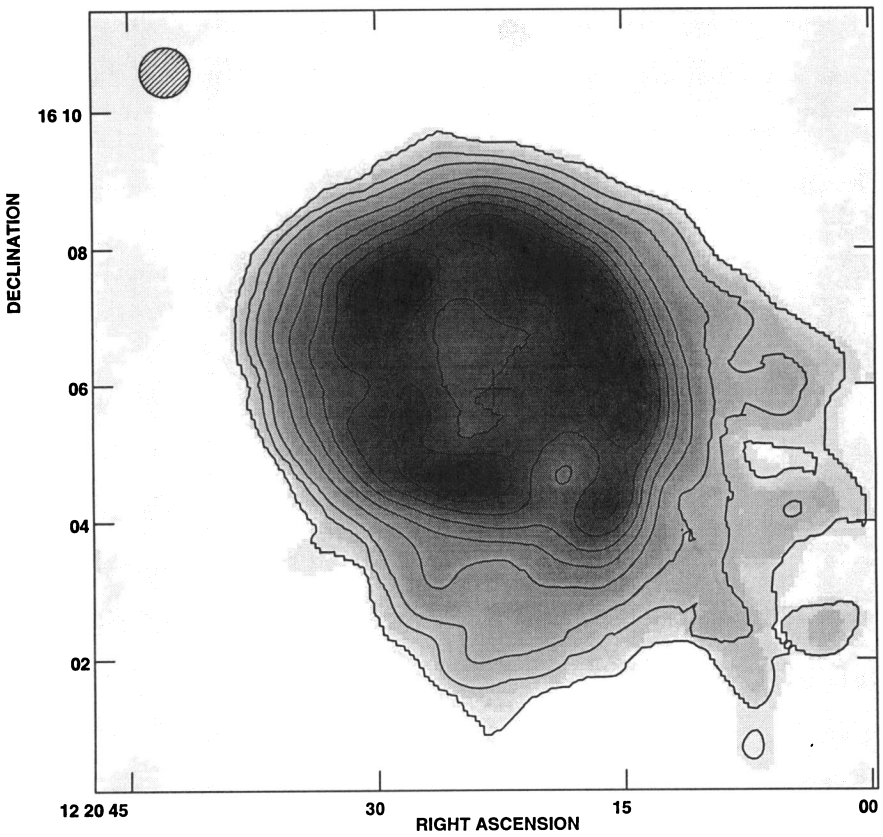

FIG. 2*c*

resolution. Channel maps at the various resolutions were used as input for the AIPS task MOMNT to calculate total H I (zeroth-moment) and velocity (first-moment) maps at each resolution. MOMNT smooths the data both spatially (over 5 pixels in our case) and in velocity (over three channels) to determine which data points to use in the calculation and masks the input maps to ensure that only smoothed points with a signal higher than 1.5 times the rms noise in the original channel maps are used in the calculation of the moment maps.

This procedure implies that gas of low brightness (and therefore not included in the mask) but spread over a large range in velocity will not be taken into account. Such an effect might occur in the centers of barred spirals, where apparent central holes in the H I distribution may be seen because the broad emission profiles fall below the threshold. To check this, we summed all the channel maps and compared the result with the zeroth-moment map. Although some differences do arise in the outer parts from noise in the channel maps, we saw no significant differences in the inner parts of the disk of the galaxy within the noise limits, so we feel we are justified in using the moment maps for the total H I distribution. In the very central regions (within about two beams from the center), where H I profiles are double peaked, the moment analysis is difficult to interpret in terms of velocity. We will discuss these regions later.

3. TOTAL H I DISTRIBUTION

In Figures 2*a*, 2*b*, and 2*c* we present the column density distribution of the H I gas in NGC 4321 at three different resolutions: 15″, 20″, and 45″. In the 20″ resolution map (Fig. 2*b*), the H I is mainly distributed along spiral arm–like structures. Between the arms, and in the center, one observes a relative deficiency of H I although the gas is detected over almost the entire disk. From CO measurements of NGC 4321 (Kenney & Young 1988; Paper I), which show a peak in the CO emission in the center and an exponential decline in the disk, it is clear that the lack of H I in the center of the galaxy does not imply a lack of gas there. This is a result that is not at all new; it has been observed in many galaxies (see, e.g., Young & Scoville 1991). A particularly interesting feature is the sharp edge to the H I distribution. The H I in fact does not extend beyond the optical radius of the galaxy, as already observed and described by Warmels (1988) and Cayatte et al. (1990). This is probably due to the location of the galaxy in the central regions of the Virgo Cluster. Most of the features just described can be easily recognized in Figure 3 (Plate 17), an overlay of the 20″ resolution H I map on a *B*-band CCD image. This image was obtained in service time at the prime focus of the 2.5 m Isaac Newton Telescope at La Palma.

Comparing the 15″ resolution map (shown in Fig. 2*a*) with the one at 20″, we see the appearance change. The arms and the large H I concentrations within them, as seen in the 20″ map, break up into smaller concentrations with a typical size of about 1 kpc and with a neutral hydrogen content of typically $3.3 \pm 0.7 \times 10^7\ M_\odot$. These concentrations follow the spiral arms as seen in optical photographs but can be seen all over the disk of the galaxy, and their location is not confined to the arms. The size of the concentrations is very similar to the beam size, which may imply that they are smaller and not resolved in

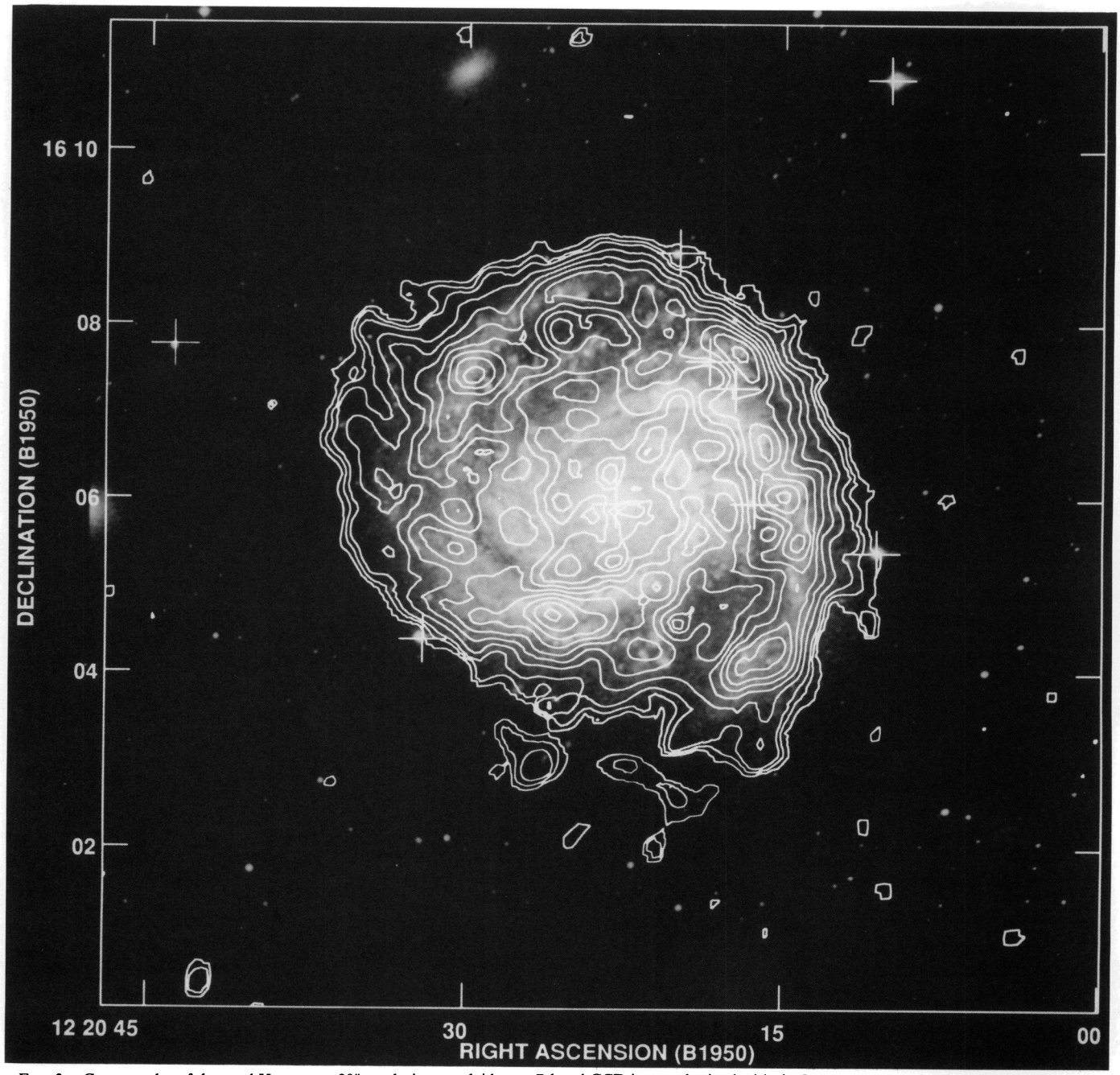

FIG. 3.—Contour plot of the total H I map at 20″ resolution overlaid on a *B*-band CCD image obtained with the Isaac Newton Telescope. Contour levels of the H I map are as in Fig. 2*b*. Extra crosses indicate star positions.

KNAPEN et al. (see 416, 568)

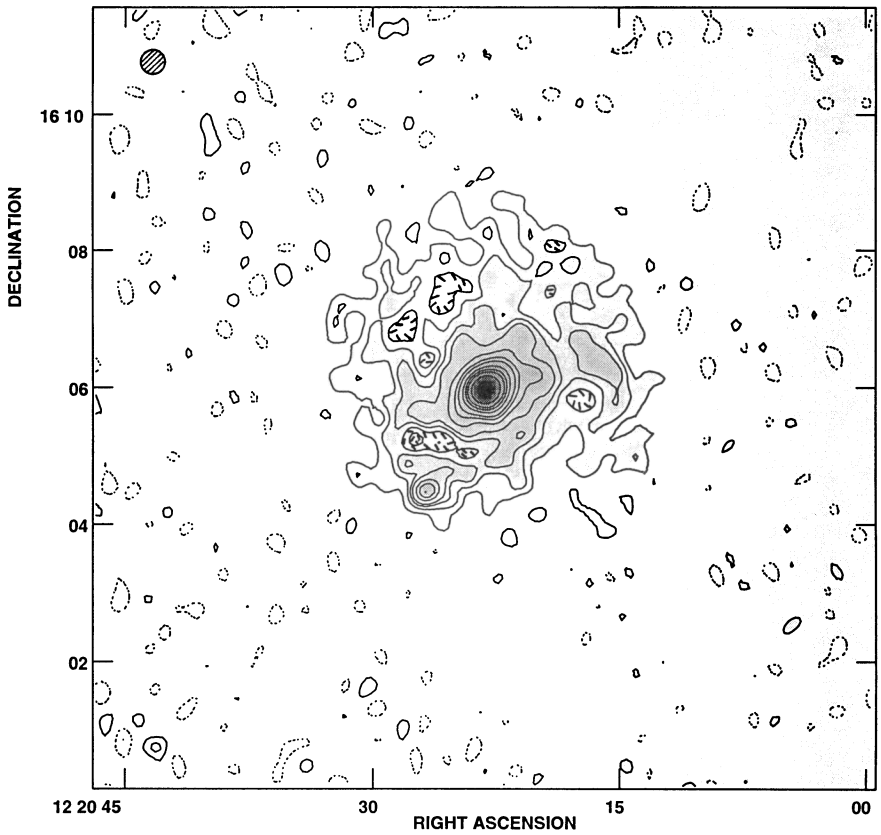

FIG. 4.—Map of the continuum emission at 21 cm of NGC 4321 at 20″ resolution (from uniform data cube). Contour levels are at −1.0, −0.5 (*dashed*), 0.5 (= 2 σ), 1.0, 1.6, 2.1, 3.1, 4.2, 5.2, 7.3, 9.4, 11.4, 15.6, and 23.4 mJy beam^{-1}. Contours are overlaid on gray-scale representation of the same image. Beam size is indicated in the upper left-hand corner.

the present observations. In a future paper, we will study the possible coincidence of the H I concentrations with bright star forming regions, combining the H I data with our Hα map of NGC 4321.

The continuum map, as subtracted from the individual channel maps, is presented in Figure 4. It shows a strong nuclear peak and an extended, faint disk where some traces of the spiral arms are visible. The strong central source and the extended disk emission were discussed by van der Kruit (1973), who could not detect the spiral arms due to the poor resolution of his observations. Van der Hulst, Crane, & Keel (1981) and Weiler et al. (1981) show from 6 cm continuum observations at 1″–5″ that the central source resolves into structures that coincide with the bright circumnuclear optical emission. Some 2′ to the SE of the nucleus, the supernova SN 1979C is visible, which has been monitored in the radio continuum by Weiler et al. (1991). In the inner 2′, the continuum image is slightly extended in the SE to NW direction, indicating the presence of the bar discussed in more detail later in this paper (§ 5).

In Figure 2*c* we show a total H I map at 45″ resolution derived from our naturally weighted channel maps. We smoothed the data cube to such a low resolution in order to compare our results with those found by Warmels (1988) and Cayatte et al. (1990), and to study the extent of the H I disk. Figure 2*c* clearly shows that the H I distribution is extended toward the SW, a result that can also be seen at low levels in the separate channel maps as shown in Figure 1*b*. This extension was detected neither by Warmels (1988) nor by Cayatte et al. (1990), probably because their sensitivity was lower. It is clear that the disk of NGC 4321 is not symmetric, making this a "lopsided" galaxy, like M101 and other galaxies as first discussed by Baldwin, Lynden-Bell, & Sancisi (1980). The velocities of the H I in the extension are somewhat lower than would be expected from a flat rotation curve. This is due to the large-scale deviation seen in the velocity field and discussed in the next section.

The explanation for the occurrence of the extension of the H I disk toward the SW of NGC 4321 is not trivial. There is a close companion, NGC 4322, at the present epoch located some 5′ toward the north of NGC 4321 at R.A.(1950.0) = $12^h20^m29^s.7$, decl.(1950.0) = 16°10′58″. This galaxy is most probably gravitationally bound and seems to be connected by a bridge in optical photographs (see, for instance, Sandage & Bedke 1988). There is no H I bridge visible in our data, either in our 45″ resolution map, or in other channel maps that were not used in the moment analysis. The extension seen in Figure 2*c* might have been caused by a close passage of the companion of NGC 4321 at some point in the history of the system, which could then also explain the deviations in the velocity field assuming that (at least part of) the gas was moved out of the plane of the galaxy. An alternative explanation might be that the observed extension is caused by ram pressure as a result of the orbit of NGC 4321 through the halo of M87 or the intergalactic medium in the Virgo Cluster, which would need to be

TABLE 3

PARAMETERS AND RESULTS FOR NGC 4321

Parameter	Value	References
Type	Sc(s)I	1
	SAB(s)bc	2
Optical size	6'.9 × 6'.2	2
	10'.0 × 9'.1	3
Optical center (1950.0)	$12^h20^m22^s.9$, 16°06'00"	1
Kinematical center (1950.0)	$12^h20^m22^s.8$, 16°05'58".2	4
Systemic velocity (heliocentric)	1570.8 ± 0.8 km s^{-1}	4
Distance	13.8 Mpc (1" = 67pc)	5
Inclination	27°	2
Position angle of major axis	153° ± 1°	6
Integrated H I flux	57.9 ± 1 Jy km s^{-1}	6
Total atomic hydrogen mass	2.5 × 10^9 $M_\odot$	6

REFERENCES.—(1) Sandage & Tammann 1987; (2) de Vaucouleurs et al. 1976; (3) Holmberg 1958; (4) this paper, determined from rotation curve fitting; (5) de Vaucouleurs 1984; (6) this paper.

toward the NE to cause the lobe in the SW. However, the morphological major axis of the H I disk appears to be almost perpendicular to the kinematic major axis of the galaxy, which means that the gas disk is not truly circular. If this ellipticity were due to a ram pressure effect it would imply movement of the galaxy along a NW-SE direction with respect to the intergalactic medium, which is nearly normal to the direction of the SW lobe, making the ram pressure explanation unlikely.

In Table 3 we summarize parameters and results for NGC 4321. We find a value for the total H I flux of $\int S\,dv = 57.9 \pm 1$ Jy km s^{-1}. The total mass of the atomic hydrogen gas can then be calculated, assuming the gas is optically thin, using the following relation:

$$M(\text{H I}) = 2.36 \times 10^5 D^2 \int S_{\text{H I}}\,dv\ ,$$

where M(H I) is expressed in solar masses, the distance D in Mpc, and the flux integral in Jy km s^{-1}. We find M(H I) = 2.6 × 10^9 $M_\odot$, at an assumed distance of 13.8 Mpc. Values for these quantities as published in the literature vary. Davies & Lewis (1973) give a value of M(H I) = 2.3 × 10^9 $M_\odot$, corrected for a distance of 13.8 Mpc. Huchtmeier, Tammann, & Wendker (1976) give a value of M(H I) = 3.3 × 10^9 $M_\odot$ (D = 13.8 Mpc). Assuming again this same distance to NGC 4321, we can determine values of M(H I) = 3.1 × 10^9 $M_\odot$ from the value of the flux integral given by Shostak (1978), whereas we can determine M(H I) = 2.2 × 10^9 $M_\odot$ from values given by both Helou et al. (1981) and Warmels (1988). All the above-mentioned studies were made with various single-beam telescopes, except for the study of Warmels, who used the WSRT. The difference between his value of $\int S\,dv$ and ours may be caused by the fact that he was missing low-order spacings, which means he could not measure structures greater than 5'.

4. KINEMATICS

4.1. *General Description*

We used the AIPS task MOMNT to calculate mean velocities over the disk of NGC 4321 (first-moment maps). Except for the inner part of the galaxy, all the separate velocity profiles are single peaked and with a shape that approaches a Gaussian. Such spectra can be handled well by MOMNT. In the inner regions, where some of the profiles are double peaked due to the effects of beam-smearing and of noncircular gas orbits, first-moment maps cannot be easily used. We will discuss this region in more detail later.

The velocity field resulting from the moment analysis (at 20" resolution) is shown in Figure 5*a*, overlaid on the total H I density map at the same resolution. As can also be seen from the channel maps, the general, underlying shape of the velocity field is the familiar pattern of a rotating galaxy disk. There are, however, notable deviations from this pattern, showing up more clearly in our velocity map than in the one published by Cayatte et al. (1990).

First of all, large-scale deviations in the velocity contours are seen in the outer SW part of the disk. There, the contours bend downward, toward higher velocities, and the observed velocities near the SW edge are consequently lower than might be expected for a simple undisturbed rotating disk. This can be seen more clearly in Figure 5*b*, where we show the velocity field of NGC 4321 at 30" resolution. This deviation is not symmetric over the galaxy; no sign of a similar shift in the contours is visible on the opposite (NE) side. As discussed in the previous section, a possible explanation for this perturbation of the velocity field (which coincides with the only region where the H I spreads significantly outside the optical disk) may be a close passage of the companion galaxy NGC 4322. The velocity field of M81 (Rots & Shane 1975) shows similar disturbances to those described here, and M81 is a notable case of a galaxy undergoing the effects of gravitational interaction with neighbor galaxies.

Further deviations in the velocity field show up as irregularities ("wiggles") in the isovelocity contours (isovels) over most of the disk. The position of the wiggles relative to the spiral arm structure indicates that they are probably signatures of density wave streaming motions, seen before in H I observations of spiral galaxies (e.g., Visser 1980; Rots et al. 1990). On the SW part of the disk it is difficult to interpret the sign and amplitude of the streaming motions due to their superposition on the large-scale deviation of the velocity field discussed in the previous paragraph. Figure 5*a* shows that in the inner galaxy (within approximately 2' from the nucleus) the strongest motions occur at the concave edges of the spiral arms, as would be expected from density wave theory assuming the spiral arms are trailing. The magnitudes of the streaming motions are between 10 and 20 km s^{-1} (deprojected 20 to 45 km s^{-1}), as estimated from relative isovel displacements.

In the central part of the galaxy, we see yet another deviation of the H I gas motions from purely rotational velocities. This effect shows up more clearly in the 30" resolution velocity field shown in Figure 5*b*. One sees that the kinematical major axis shows a change in position angle with radius. The skewing in the isovels near the center of a galaxy can be caused by a nonaxisymmetric potential in the underlying mass distribution, e.g., a bar. This idea has been supported theoretically (e.g., Roberts, Huntley, & van Albada 1979; Sanders & Tubbs 1980) and observed in several barred galaxies, both in the optical (e.g., Peterson et al. 1978) and in H I (e.g., Sancisi et al. 1979; Bosma 1981a, b; Gottesman et al. 1984; Ball 1986; Ondrechen & van der Hulst 1989; Ondrechen et al. 1989). Distortions in the velocity field similar to those considered here could also be caused by an intrinsic warp in the H I disk (see Bosma 1981b for a discussion), but the fact that the kinematical major axis is not perpendicular to the minor axis near the center of the galaxy does not favor an explanation in terms of such a warp. Furthermore, we shall see later (§ 5) that there is evidence from

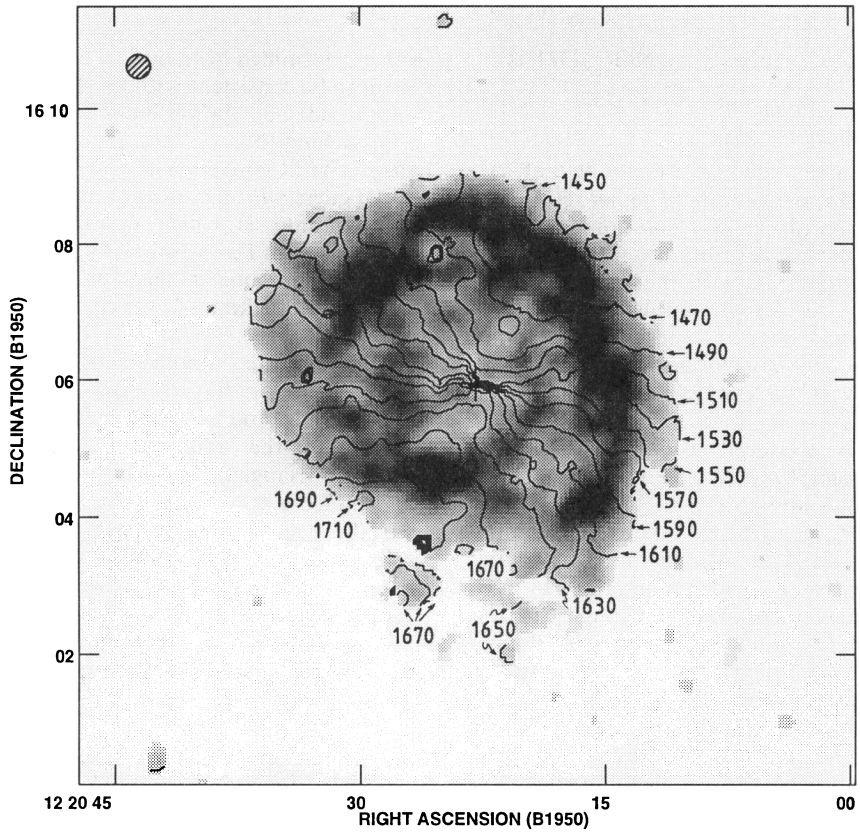

FIG. 5a

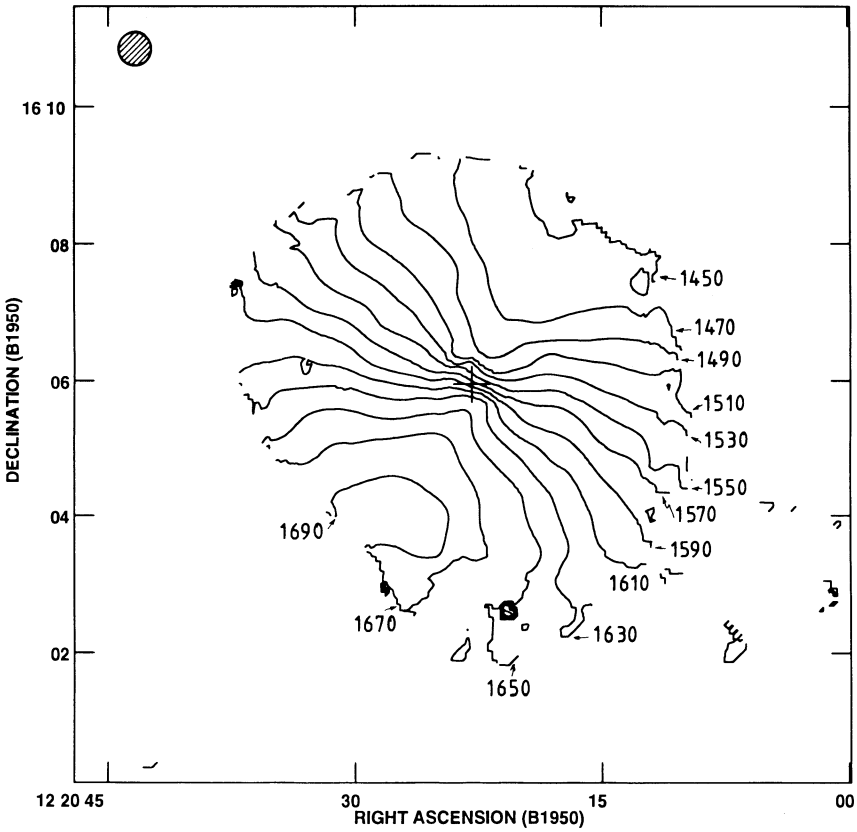

FIG. 5b

FIG. 5.—(*a*) Velocity field at 20″ resolution. Contours are from 1430 to 1710 km s^{-1} in steps of 20 km s^{-1} (heliocentric velocities). This map is shown overlaid on a gray-scale representation of the total H I distribution at 20″ (see Fig. 2*b*). Cross represents optical center. Beam size is indicated in the upper left-hand corner. (*b*) As Fig. 5a, but as determined from the 30″ resolution data.

optical and near-infrared observations that NGC 4321 is in fact a barred spiral.

4.2. *Rotation curve*

We derive the rotation curve from our velocity field at 15″, 30″, and 45″ resolution. To do so we combine higher resolution in the inner parts of the galaxy (using 15″ resolution data) with higher sensitivity in the outer parts (using the 45″ resolution data). We then compare our results with those of Guhathakurta et al. (1988, hereafter GGKB), who published a study of the rotation curves of the Virgo Cluster spiral sample described by Cayatte et al. (1990), including NGC 4321. The data used by GGKB for NGC 4321 were VLA observations with a resolution of 45″ × 42″.

Our rotation curve was produced using the procedure described in detail by Begeman (1989). We used a version of the GIPSY program ROTCUR running in a SUN environment and kindly made available to us by A. H. Broeils. In this procedure, the rotation curve is derived after dividing the galaxy into a set of concentric rings, each of which is described by a set of values of i, ϕ, and v_C, where i is the inclination angle, ϕ is the position angle of the major axis, and v_C is the rotation velocity. Values for these parameters in each ring are fitted using a least-squares algorithm. Data points are weighted by $|\cos(\theta)|$, where θ is the azimuthal angle from the major axis. Data points within 20° of the minor axis were not used in the fits. Using reasonable values for the parameters as initial guesses of i, ϕ, v_C, the systemic velocity v_{sys}, and the position (x, y) of the center, we first determined values for the systemic velocity and the position of the dynamical center of the galaxy, which are in good agreement with values published in the literature.

Since NGC 4321 is a galaxy with a low inclination angle, it is impossible in practice to fit both v_C and i, and we therefore opted to keep the inclination angle fixed. We chose $i = 27°$ (a value determined from optical isophotes; de Vaucouleurs et al. 1976) to be consistent with GGKB, who also fixed i at 27°. We then fitted the rotation curve for the whole disk, and for the approaching (N) and receding (S) halves of the galaxy separately. The fit converges to the same solution if we start from initial guesses for the fitted parmeters that are not in agreement with the data set, which increases our confidence in the solution. Fits with i as a free parameter give rotation curves with unrealistic parameters (such as apparent rotation velocities of well over 1000 km s^{-1}) which therefore cannot be taken seriously.

The resulting combined rotation curve for NGC 4321 is shown in Figure 6 (shown are the fits for the whole disk, and approaching and receding sides separately), where we have also plotted the rotation curve derived by GGKB, denoted by the open triangles. The first part of the curve (out to 95″) was derived from our 15″ resolution data. The points in the middle part (between 95″ and 160″) are derived from the 30″ resolution velocity field, and the outer points (from 165″ outward) from the 45″ resolution velocity field. We have combined the data in such a way as to obtain the best possible compromise between high resolution and high sensitivity. The error bars shown around the points in Figure 6 are the errors from the least-squares fitting procedure. The errors introduced by fixing the inclination angle may be considerably larger. For instance, changing the value of i from 27° to 30° (a value derived by Warmels 1988 from his Westerbork observations) would cause a change in the fitted rotation velocities of about 18 km s^{-1}.

Comparing our rotation curve with the one derived by GGKB, we note first of all that our curve rises more steeply near the center. This confirms the view of GGKB that beam-smearing effects are responsible for the relatively slow rise of the rotation curves they derived for their sample of Virgo Cluster spirals. The canonical synthetic curves for Sc galaxies

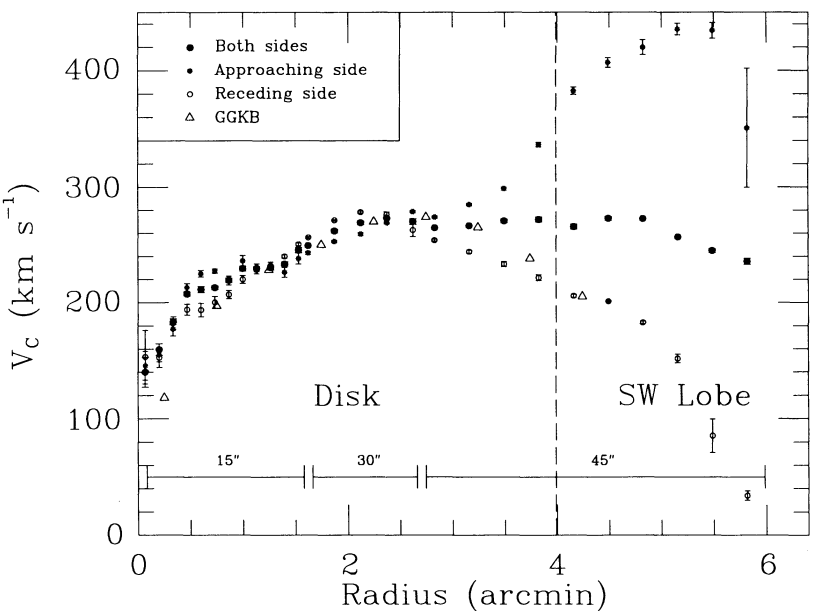

FIG. 6.—Derived rotation curve (whole disk: *full dots*; approaching side only: *stars*; receding side: *open circles*) compared with the rotation curve from Guhathakurta et al. (1988; *open triangles*). The vertical dashed line indicates the approximate extent of the H I disk at 45″ resolution; the part of the curve to the right of this line is derived from H I in the SW lobe and cannot be interpreted as disk rotation. The horizontal bars at the bottom of the figure indicate which data set was used to derive the rotation curve in a certain range of radius. High-resolution (15″) data were used for the inner part, low-resolution (45″) data for the outer part, and 30″ resolution data for the intermediate part.

as given by Rubin et al. (1985) rise more steeply than GGKB's H I curve in the central parts, and our rotation curve as determined from higher resolution data approaches the synthetic curves more closely. This interpretation is supported by the observed CO spectral profile on the nucleus obtained in Paper I. This profile, measured within a beam of half-power width 15″, has a FWHM of 145 km s^{-1}. Assuming this to be caused by rotation, and deprojecting into the plane of the galaxy using $i = 27°$, we find a corresponding velocity range of 320 km s^{-1}. This value would correspond to a rapidly rising rotation curve, rising in fact slightly faster than the one derived here, comparing the CO value with what we see at ~7″.5 from the nucleus in Figure 6 (where of course there is some beam-smearing effect).

Comparing the extent of the rotation curve with the total H I distribution at low resolution (Fig. 2*c*) it becomes clear that the rotation curve as a description of the circular motions over the disk of the galaxy can only be valid within a radius of 4′, indicated in Figure 6 with the dashed vertical line. Beyond that radius, only emission from the extension in the H I disk on the SW is used as input for the fitting routine. The rotation curve will therefore describe only the motions of that part, not disk motions, and cannot be easily interpreted. We show this part of the rotation curve for comparison only in Figure 6. As can be seen in Figure 5*b*, large-scale deviations in the outer parts of the disk are already influencing the determination of the rotation curve just inside the radius of 4′.

Up to a radius of slightly more than 3′, the GGKB rotation curve agrees well with ours. However, GGKB find from their two outermost data points that the rotation curve is falling, whereas we find that it stays more or less constant. The difference might be due to the fact that different methods were used to determine the curves, or to the fact that the sensitivity is higher in our new data than in GGKB's data. We do confirm that the derived curve for the approaching side of the galaxy rises out to the full extent of the H I disk whereas the one for the receding side falls after reaching a maximum rotation velocity at a radius of slightly more than 2′. This observational difference is caused by the large-scale deviation from circular velocities in the outer parts of the disk on the SW side, which was discussed before. It is noteworthy that fitting the whole disk beyond 3′ yields an apparently classically behaved flat curve, but this does not (for this galaxy) indicate true circular motion and should not, of course, be used to infer a mass distribution. We also observe differences of up to about 30 km s^{-1} between the "rotation velocities" as derived from the approaching and receding halves of the galaxy between 1′ and 3′ in radius. These differences are probably due to noncircular motions occurring in the regions of the spiral arms.

5. THE BAR IN NGC 4321

In Figure 7 (Plate 18) we show our 20″ resolution total H I map overlaid on an Hα image of NGC 4321. The Hα image shown here is a mosaic of four fields observed with the TAURUS instrument in imaging mode on the 4.2 m William Herschel Telescope on La Palma. The original resolution is 0″.8 (seeing value, well sampled with the 0.27 $arcsec^2$ pixels), although in Figure 7 this appears degraded due to the limits of reproduction. The total extent of the Hα map is about 7′ square (or about 1880 × 1850 pixels), and covers all the star forming regions in the disk of NGC 4321. The overlay shows that the Hα emission outlines the spiral arms seen in the H I and optical continuum images. A pattern typical of barred spiral galaxies is seen in the Hα image: there is hardly any massive star formation in the bar region, whereas strong Hα emission is seen at the ends of the bar ("cusps"), implying strong massive star formation activity there. A more detailed comparison of Hα emission and H I column density will be made in a future paper.

In Figure 8 (Plate 19) we present a CCD image in the near-infrared *I*-band. The image was taken in service time at the prime focus of the 2.5 m Isaac Newton Telescope at the Observatorio del Roque de los Muchachos, La Palma. The total field size is about 11′, pixel size is 0″.56, and the seeing was better than 1″ FWHM. The central region of the *I*-band image shows an elongated distribution of light, extending roughly in the SE to NW direction, and about 2′ long. This optical bar coincides with the position and extent expected for a barlike structure from the H I kinematics. The same structure is more clearly seen in an image in the near-infrared *H*-band (R. F. Peletier, private communication), taken with the SONIC array at the Mount Hopkins 24 inch (61 cm) telescope; the instrumentation and data reduction procedures are described by Peletier & Willner (1991). Although the bar does not show up prominently in optical images in blue or visible passbands, it does show its influence on the old stellar population and is visible in the NIR. Pierce (1986) published an *I*-band image where the bar is visible, and Pogge (1989) mentions NIR mapping as a possible way to detect a bar in NGC 4321, which he expects from his narrow-band observations of the star formation in the central region.

In Figure 9 we show a set of position-velocity diagrams along lines parallel to the minor axis, as drawn from our 20″ resolution data set. These lines are separated by 8″ which corresponds to $\frac{2}{5}$ of a beam. Pure disk rotation would show up as a completely flat position-velocity diagram along the minor axis, turning into a V-shape as one moves away from the minor axis. In Figure 9 we see that the profile along the minor axis (*middle panel*) shows a flat general shape, with some wiggles in the left and right wings which are probably due to streaming motions near the spiral arms. In the central part, extensions with positive and negative velocities with respect to the systemic velocity are seen. These appear in the region where the individual H I profiles exhibit double profiles, and thus where the moment analysis will not yield valid single-component velocities.

In Figure 9 one also sees that there are two regions, symmetrically placed around the minor axis, which show positive and negative excess velocities (with respect to the v_{sys}). Maximum residuals (absolute values) in both regions are of order 50 km s^{-1}. The residuals occur at the positions where the isovels show their skew, and indicate the presence of the non-axisymmetric potential. Excess negative velocities occur at the north, or approaching side, and excess positive velocities at the south or receding side. This means that we see the gas streaming along the bar, which moves in the same direction as the disk, but with higher apparent rotational velocities. In Paper I we presented evidence that the spiral arms are trailing, and that the NE side of NGC 4321 is in fact the near side. The gas streaming along the bar is thus moving in a counterclockwise direction. One must keep in mind that the 20″ beam introduces beam smearing, and that the panels, separated by 8″, are not independent. The overall picture, of excess positive velocities on the receding side and excess negative velocities on the approaching side, is, however, real.

Comparing this picture of gas flows with theoretical predictions, we see an interesting qualitative agreement. As shown,

PLATE 18

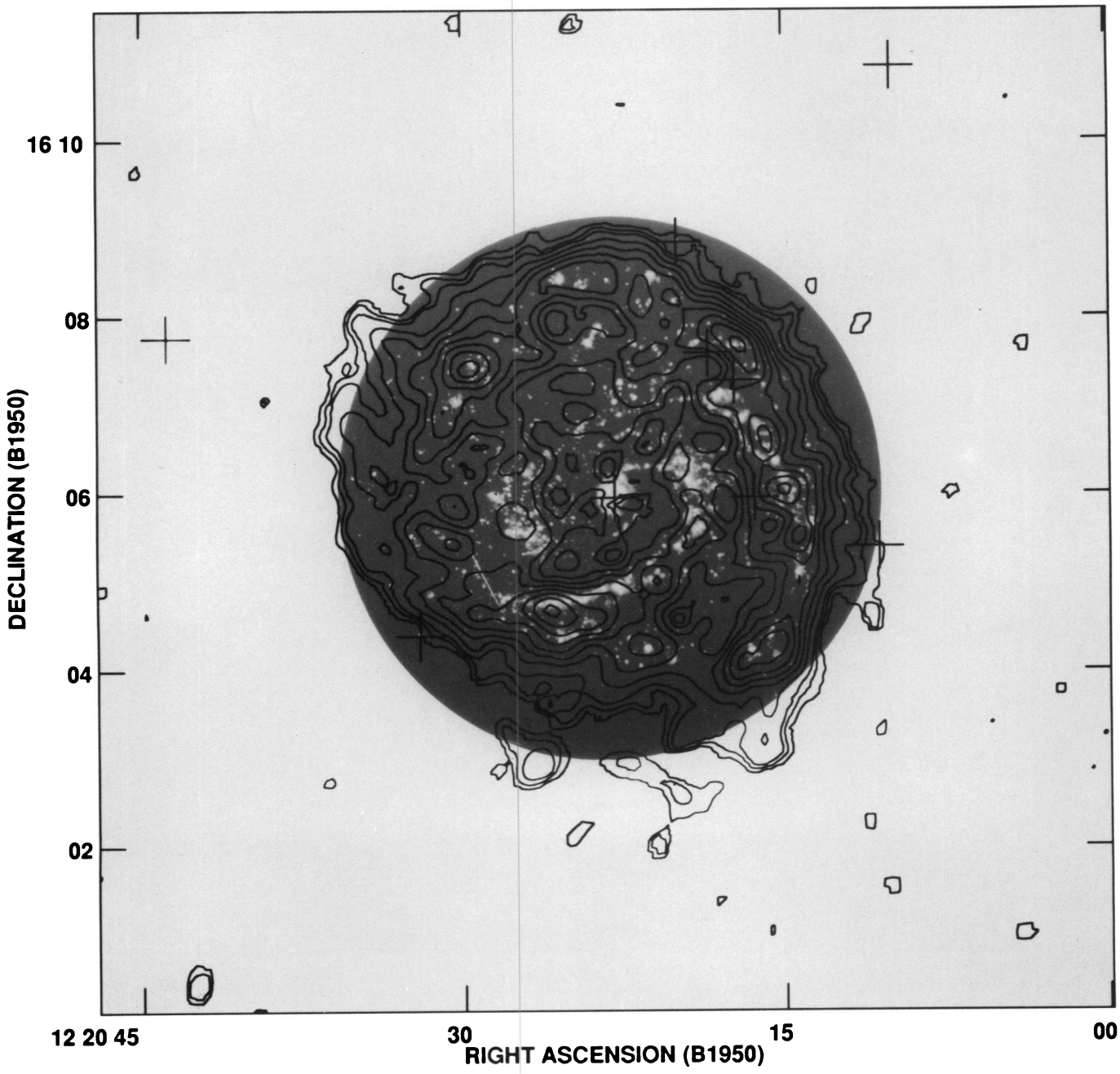

FIG. 7.—Contour plot of the total H I map at 20″ resolution overlaid on an Hα image of NGC 4321, obtained with the William Herschel Telescope. Contour levels of H I map are as in Fig. 2*b*.

KNAPEN et al. (see 416, 573)

FIG. 8.—*I*-band CCD image of NGC 4321 obtained with the Isaac Newton Telescope. North is at the top; east to the left.

KNAPEN et al. (see 416, 573)

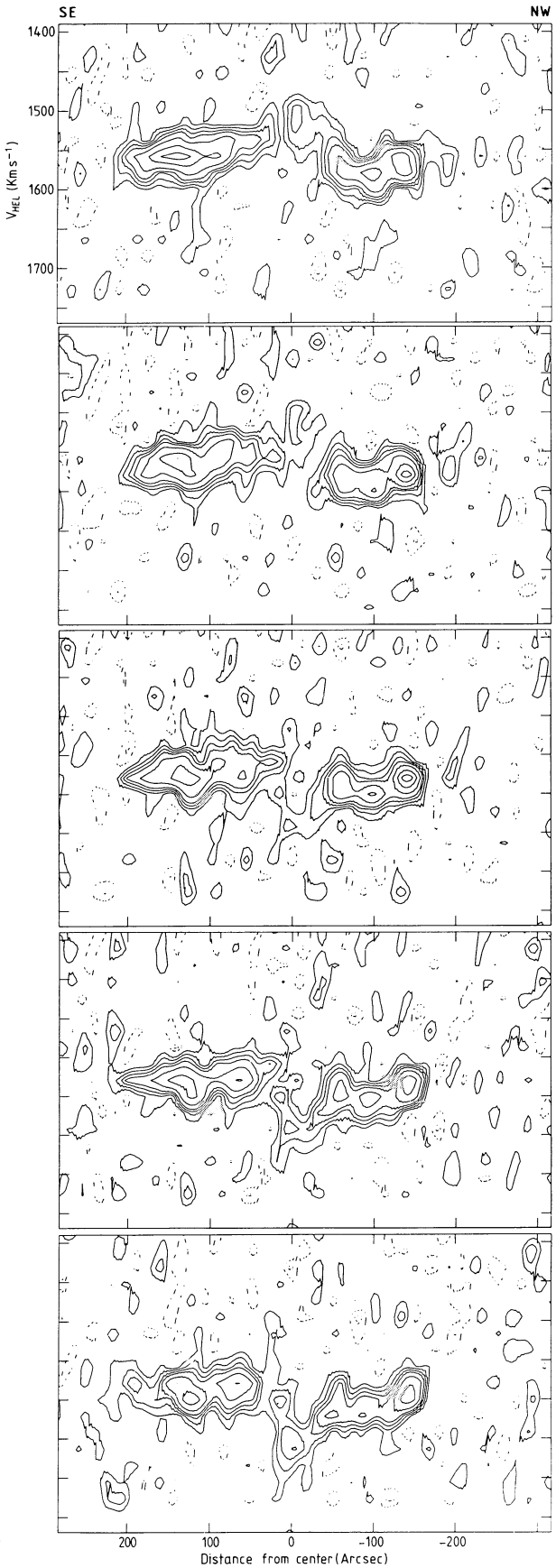

e.g., by Roberts et al. (1979) or more recently by Athanassoula (1991, 1992a, b), gas orbits at radii corresponding to the outer part of a stellar bar are elongated along the principal axis of the bar and would give rise to the excess velocities seen in our Figure 9. Velocities change abruptly at shock fronts offset from the major axis of the bar, which coincide with dust lanes, seen in optical images. Although the angular resolution in the velocity information at our disposal for the central regions is not high, the qualitative agreement of the H I and optical observations with theoretical bar models is clear.

6. CONCLUSIONS

We have observed the grand design spiral galaxy NGC 4321 with the VLA and produced data cubes with angular resolutions ranging from 13″.31 × 12″.73 to 45″. The main results can be summarized as follows:

1. We detect H I over the whole disk of the galaxy. The distribution shows concentrations over the main spiral arms, and a depression in the center. Over most of the disk, the H I is limited to the radial extent of the optical disk. This is all in agreement with previously published H I observations at lower resolution.

2. We have discovered a large though faint extension of the H I gas on the SW side of the disk, making NGC 4321 asymmetric in atomic hydrogen ("lopsided"). The velocity field shows large-scale deviations from circular motions in the same region. The extension and the velocity deviations may well be due to a previous close passage of the companion galaxy NGC 4322, although they might just possibly be caused by ram pressure as a result of the orbit of NGC 4321 through the Virgo Cluster.

3. At 15″ resolution, the H I is observed in clumps of typical total mass of $3.3 \pm 0.7 \times 10^7\ M_\odot$ which may, however, not be resolved. They have physical sizes of 1 kpc or smaller. The clumps are not confined to the arms, but are also seen in the interarm disk.

4. From our combined data set, we have derived a rotation curve for NGC 4321, which agrees reasonably well with previously published determinations. The inner part of our curve rises more steeply, due to the higher resolution of the present observations. The outer part of the curve, as derived from the 30″ and 45″ resolution velocity fields shows a rising slope for the approaching side of the galaxy, whereas the curve for the receding side falls after reaching a maximum. Although the average curve for the whole disk shows an almost constant velocity in the outer parts, beyond 3′ from the center it cannot be used as a true measure of circular motion.

5. Density wave streaming motions with projected amplitudes of 10–20 km s^{-1} (deprojected 20–45 km s^{-1}) appear in the velocity field across the spiral arms.

6. In the central region of NGC 4321, skewing of the velocity contours indicates the presence of a nonaxisymmetric potential. A bar is seen on near-infrared CCD images, and the dis-

FIG. 9.—Panel of five position-velocity diagrams along and parallel to the minor axis at 20″ resolution. Middle panel shows cut along the minor axis, two panels at the top show cuts parallel to and north of the minor axis, and two panels at the bottom show similar cuts south of the minor axis. Separation between cuts is 8″ or $\frac{2}{5}$ of a beam (FWHM). Contour levels are at −2.1 (*dashed*), 2.1 (= 2 σ), 4.2, 7.3, 10.5, and 15.7 K. Note that higher velocities are plotted toward the bottom. Grid labeling is the same for all panels.

tribution of massive star forming regions, as seen in an Hα map, also is consistent with the presence of a bar. From these observations, we conclude that NGC 4321 is a barred galaxy, although the bar is not particularly strong and hardly shows up in images taken in blue or visible bands.

7. Deviations from circular motions allow us to determine the direction of the gas flow around the bar. From the kinematics we can deduce that the gas moves counterclockwise around the bar, i.e., in the same direction as the rotation of the galactic disk. This observation agrees qualitatively with theoretical models describing gas flows in and around bars.

E. Brinks gave invaluable help during the observation and data reduction phase of this project. A. Szomoru and J. M. van der Hulst helped by giving their opinions on many aspects of the data reduction and interpretation of the data. We acknowledge illuminating discussions with R. Sancisi, F. Combes, and J. D. P. Kenney. A. H. Broeils supplied us with a new version of the rotation curve program ROTCUR. R. F. Peletier let us have a look at his *H*-band image of NGC 4321. We thank R. Terlevich and M. J. Sempere for their help in obtaining the optical service observations. We are grateful to the anonymous referee for a number of constructive suggestions which have aided us in improving the paper. The National Radio Astronomy Observatory is operated by Associated Universities, Inc., under cooperative agreement with the National Science Foundation. The William Herschel and Isaac Newton Telescopes are operated on the island of La Palma by the Royal Greenwich Observatory in the Spanish Observatorio del Roque de los Muchachos of the Instituto de Astrofísica de Canarias. This work was partially supported by the Spanish DGICYT (Dirección General de investigación Científica y Técnica) grant PB89-0510.

REFERENCES

Allen, R. J., Atherton, P. D., & Tilanus, R. P. J. 1986, Nature, 319, 296
Arsenault, R., Boulesteix, J., Georgelin, Y., & Roy, J.-R. 1988, A&A, 200, 29
Athanassoula, E. 1991, in Dynamics of Disc Galaxies, ed. B. Sundelius (Göteborg: Dept. of Astronomy/Astrophysics, Göteburg University & Chalmers Inst. of Technology), 149
———. 1992a, MNRAS, 259, 328
———. 1992b, MNRAS, 259, 345
Baldwin, J. E., Lynden-Bell, D., & Sancisi, R. 1980, MNRAS, 193, 313
Ball, R. 1986, ApJ, 307, 453
Begeman, K. G. 1989, A&A, 223, 47
Bosma, A. 1981a, AJ, 86, 1791
———. 1981b, AJ, 86, 1825
Cayatte, V., van Gorkom, J. H., Balkowski, C., & Kotanyi, C. G. 1990, AJ, 100, 604
Cepa, J., & Beckman, J. E. 1990a, ApJ, 349, 497
———. 1990b, A&AS, 83, 211
Cepa, J., Beckman, J. E., Knapen, J. H., Nakai, N., & Kuno, N. 1992, AJ, 103, 429 (Paper I)
Clark, B. G. 1980, A&A, 89, 377
Clemens, D. P. 1985, ApJ, 295, 422
Davies, R. D., & Lewis, B. M. 1973, MNRAS, 165, 231
de Vaucouleurs, G. 1984, in The Virgo Cluster, ed. O. G. Richter & B. Binggeli (Garching: ESO), 413
de Vaucouleurs, G., de Vaucouleurs, A., & Corwin, H. G. 1976, Second Reference Catalogue of Bright Galaxies (Austin: University of Texas Press) (RC2)
Gottesman, S. T., Ball, R., Hunter, J. H., & Huntley, J. M. 1984, ApJ, 286, 471
Guhathakurta, P., van Gorkom, J. H., Kotanyi, C. G., & Balkowski, C. 1988, AJ, 96, 851 (GGKB)
Helou, G., Giovanardi, C., Salpeter, E. E., & Krumm, N. 1981, ApJS, 46, 267
Holmberg, E. 1958, Medd. Lunds. Astron. Obs., Ser. II, No. 136
Huchtmeier, W. K., Tammann, G. A., & Wendker, H. J. 1976, A&A, 46, 381
Ichikawa, T., Nakano, M., Tanaka, Y. D., Saito, M., Nakai, N., Sofue, Y., & Kaifu, N. 1985, PASJ, 37, 439
Kenney, J. D., & Young, J. S. 1988, ApJS, 66, 261
Knapen, J. H., Beckman, J. E., Cepa, J., van der Hulst, J. M., & Rand, R. J. 1992, ApJ, 385, L37
Kotanyi, C. G. 1980, A&AS, 41, 421
Ondrechen, M. P., & van der Hulst, J. M. 1989, ApJ, 342, 29
Ondrechen, M. P., van der Hulst, J. M., & Hummel, E. 1989, ApJ, 342, 39
Peletier, R. F., & Willner, S. P. 1991, ApJ, 382, 382
Pence, W. D., Taylor, K., Freeman, K. C., de Vaucouleurs, G., & Atherton, P. 1988, ApJ, 326, 564
Peterson, C. J., Rubin, V. C., Ford, W. Kent, & Thonnard, N. 1978, ApJ, 219, 31
Pierce, M. J. 1986, AJ, 92, 385
Pogge, R. W. 1989, ApJS, 71, 433
Roberts, W. W., Huntley, J. M., & van Albada, G. D. 1979, ApJ, 233, 67
Rots, A. H., Bosma, A., van der Hulst, J. M., Athanassoula, E., & Crane, P. C. 1990, AJ, 100, 387
Rots, A. H., & Shane, W. W. 1975, A&A, 45, 25
Rubin, V. C., Burstein, D., Ford, W. Kent, & Thonnard, N. 1985, ApJ, 289, 81
Sancisi, R., Allen, R. J., & Sullivan, W. T. 1979, A&A, 78, 217
Sandage, A., & Bedke, J. 1988, Atlas of Galaxies Useful for Measuring the Cosmological Distance Scale (NASA SP-496), 35
Sandage, A., & Tammann, G. A. 1987, A Revised Shapley-Ames Catalog of Bright Galaxies (2d ed.; Washington: Carnegie Institution of Washington)
Sanders, R. H., & Tubbs, A. D. 1980, ApJ, 235, 803
Scoville, N. Z., & Young, J. S. 1983, ApJ, 265, 148
Shostak, G. S. 1978, A&A, 68, 321
Tilanus, R. P. J., & Allen, R. J. 1989, ApJ, 339, L57
———. 1991, A&A, 244, 8
van der Hulst, J. M., Crane, P. C., & Keel, W. C. 1981, AJ, 86, 1175
van der Kruit, P. C. 1973, A&A, 29, 249
Visser, H. C. D. 1980, A&A, 88, 159
Warmels, R. H. 1988, A&AS, 72, 19
Weiler, K. W., van der Hulst, J. M., Sramek, R. A., & Panagia, N. 1981, ApJ, 243, L151
Weiler, K. W., Van Dyk, S. D., Panagia, N., Sramek, R. A., & Discenna, J. L. 1991, ApJ, 380, 161
Young, J. S., & Scoville, N. Z. 1991, ARA&A, 29, 581